Experimental and Modeling Uncertainty Considerations for Determining the First Item Ignited in a Compartment Using a Bayesian Method

J. M. Cabrera
Department of Mechanical Engineering,
The University of Texas at Austin,
Austin, TX 78712
e-mail: janmichael.cabrera@mail.utexas.com

R. D. Moser
Institute for Computational Engineering and Sciences,
The University of Texas at Austin,
Austin, TX 78712
e-mail: rmoser@ices.utexas.edu

O. A. Ezekoye[1]
Department of Mechanical Engineering,
The University of Texas at Austin,
Austin, TX 78712
e-mail: dezekoye@mail.utexas.edu

Fire scene reconstruction and determining the fire evolution (i.e., item-to-item ignition events) using the postfire compartment is an extremely difficult task because of the time-integrated nature of the observed damages. Bayesian methods are ideal for making inferences amongst hypotheses given observations and are able to naturally incorporate uncertainties. A Bayesian methodology for determining probabilities to items that may have initiated the fire in a compartment from damage signatures is developed. Exercise of this methodology requires uncertainty quantification of these damage signatures. A simple compartment configuration was used to quantify the uncertainty in damage predictions by FIRE DYNAMICS SIMULATOR (FDS) *and, a compartment evolution program,* JT-RISK *as compared to experimentally derived damage signatures. Surrogate sensors spaced within the compartment use heat flux data collected over the course of the simulations to inform damage models. Experimental repeatability showed up to 4% uncertainty in damage signatures between replicates. Uncertainties for* FDS *and* JT-RISK *ranged from 12% up to 32% when compared to experimental damages. Separately, the evolution physics of a simple three-fuel-package problem with surrogate damage sensors were characterized in a compartment using experimental data,* FDS, *and* JT-RISK *predictions. A simple ignition model was used for each of the fuel packages. The Bayesian methodology was exercised using the damage signatures collected, cycling through each of the three fuel packages, and combined with the previously quantified uncertainties. Only reconstruction using experimental data was able to confidently predict the true hypothesis from the three scenarios.* [DOI: 10.1115/1.4052796]

1 Introduction

The processes associated with fire evolution within a compartment from ignition to the extinguished state involve complex, coupled multiscale, multiphysics phenomena that are difficult to model in detail. The fire evolution process involves heat transfer, in the reacting and complex fire flow field, to solid fuel packages in the compartment. Changes in ventilation condition of the compartment, the activation of smoke control systems and sprinklers, etc., add further complexity to analyzing fire compartment problems. Significant portions of the information pertaining to the fire evolution are destroyed because of the fire itself. The remaining information available in the form of fire signatures (e.g., gypsum wallboard calcination, plastic deformation, soot deposition, etc.) help aid fire and arson investigators in determining fire origin and cause. Fire models such as FIRE DYNAMICS SIMULATOR (FDS) and CONSOLIDATED MODEL OF FIRE AND SMOKE TRANSPORT can help augment the information available to the investigator.

NFPA 921, Guide for Fire and Explosion Investigations aims to reduce biases and standardize the investigation process by providing guidance to fire investigators for creating and testing of fire scene hypotheses [1]. The hypothesis space is a high-dimensional space consisting of compartment and fuel package geometries, ventilation conditions, material compositions, and possible initiation scenarios. When a fire investigator arrives at the fire scene, narrowing down of the hypothesis space happens naturally and automatically. This inference process is one that shifts probability mass from all possible hypotheses about the compartment without having observed any data, to hypotheses that are consistent with the observations made. After the initial intuitive assessments, the fire investigator generally uses prior knowledge (i.e., experience) and intuition about the physical processes to further reduce the hypothesis space. Fire scene evidence in the form of postfire damage, witness statements, sensor readings, video, etc., available to the fire investigator should support the hypothesis reduction process. However, high-quality evidence such as video and sensor readings are not always available.

Shortcomings in statistically weighing evidence used in prosecution for the forensic sciences have been reported by the U.S. National Academies recently [2]. Fire origin determination, without which cause cannot be determined, also requires proper weighing of evidence from the fire scene. Gorbett and Chapdelaine use NFPA 921 as a guide for arranging origin determination subprocesses such that they are more consistent with the scientific method. This arrangement is meant to help the fire investigator form and test hypotheses about the fire scene [3]. Other methods for determining the area of origin, such as the origin matrix method [4], still require systematic evaluation on the efficacy of the methodology [5]. Postfire, fire patterns, "visible or measurable physical changes, or identifiable shapes, formed by a fire effect or group of fire effects" [5], have been used to link observed damages to heat sources but report large variability [6–8]. Preflashover fire pattern uncertainties have also been shown to increase with increasing fuel complexity [9].

Stauffer provides a comprehensive review of fire research in the fire community ranging from predictive models to new ignition scenarios [10]. Most compartment scale experiments reported were conducted with single fires or scenarios where the fuel

[1]Corresponding author.

Manuscript received April 14, 2021; final manuscript received October 4, 2021; published online November 17, 2021. Assoc. Editor: Joshua Kaizer.

source would generate uncertain, time-varying heat release rate (HRR) curves. Bayesian methods, which make explicit use of uncertainty in the observed quantities and prior information, are well suited to quantifying fire scene hypotheses. These methods have been applied to a number of fire problems but have yet to address quantifying possible fire scene hypotheses for area determination [11–18]. Recently, Cabrera et al. have demonstrated the need to account for uncertainty in origin determination for three-fuel-package scenarios within an electronically controlled and actuated fire compartment given the time history of heat fluxes at surrogate sensors located throughout the compartment [19]. This work builds upon this concept and aims to quantify fire scene hypotheses given postfire damage signatures in the compartment while taking into account the associated uncertainties. The Bayesian framework for statistically weighing fire scene hypotheses is introduced in Sec. 2. Details of a simple point-source compartment fire evolution model, JT-RISK, coupled with a simple critical heat flux ignition criterion are discussed in Sec. 3. Also discussed in this section is the use of FDS as a compartment evolution fire model. Discussion of the time incident heat flux history at surrogate sensors converted into damage metrics is presented in Sec. 3.4. The uncertainty of these damage metrics for JT-RISK and FDS compared to experimental results is derived in Sec. 4 for a simple, single fire scenario. Application of the Bayesian methodology for weighing the fire scene hypotheses given the uncertainty in damage metrics is discussed in Sec. 6. An instrumented and electronically actuated experimental test compartment was used for the experiments described in Secs. 4 and 5.

2 Bayesian Framework

A fire investigator analyzing a postfire compartment may like to know the area of origin of the fire from possible hypothetical locations. The investigator would then like to use the available data and any prior knowledge to test the different hypotheses to elicit the true area of origin. A simplified scenario of the possible hypotheses is shown in Fig. 1.

To simplify the inferential process, it can be assumed that the thermophysical and geometrical properties describing the compartment, ignited items, surrogate sensors, etc., are known. The question then reduces to which of the possible objects in the compartment (which hypothesis) initiated the fire. This can be expressed using Bayes' theorem as

$$P(H_i|D) = \frac{P(H_i)P(D|H_i)}{\sum_{l=1}^{m} P(H_l)P(D|H_l)} \tag{1}$$

where $P(H_i)$ is the probability one would apply to each of the hypotheses prior to observing the data (but after a cursory review

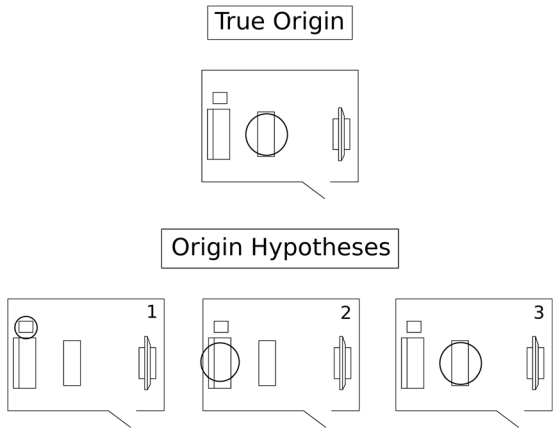

Fig. 1 Fire investigation scenario showing the true fire origin and origin hypotheses for a toy case

of the compartment), $P(D|H_i)$ is the likelihood function, which will be shown to represent the model misfit given particular hypotheses (i.e., the misfit in predicted damage for a hypothesis to the observed damage), and $P(H_i|D)$ represents how one would update one's prior beliefs $P(H_i)$ after having observed the data. Note here that the likelihood and therefore the posterior are implicitly conditioned on the type of model used.

The prior is a discrete distribution enumerating the probability that a particular area in the compartment initiated the fire

$$P(H_i) = h_i; \quad \sum_{i=1}^{m} P(H_i) = 1 \tag{2}$$

The likelihood is derived by specifying a statistical model

$$x_j = \hat{x}_{ij} + e_j; \quad e_j \sim N(0, \sigma_j^2) \tag{3}$$

It states that the true observed damage x_j at sensor j is assumed to be the predicted damage for sensor j given hypothesis i, $\hat{x}_{ij}$, with mean zero Gaussian noise with variance σ_j^2. The σ_j^2 term does not depend on the hypothesis chosen as it is a value that can be found when evaluating the uncertainty of the model prediction given a known true configuration. Assuming that the surrogate sensor data are independent and identically distributed (iid), the full likelihood for hypothesis, i, is

$$P(D|H_i) = \prod_{j=1}^{J} P(x_j|\hat{x}_{ij}, \sigma_j^2, H_i) \tag{4}$$

$$= \left(\frac{1}{2\pi}\right)^{J/2} \exp\left[-\frac{1}{2}\sum_{j=1}^{J}\frac{(x_j - \hat{x}_{ij})^2}{\sigma_j^2}\right] \prod_{j=1}^{J}\left(\frac{1}{\sigma_j^2}\right) \tag{5}$$

Equations (2) and (4) are substituted into Eq. (1) and reduce to

$$P(H_i|D) = \frac{h_i \cdot \exp\left[-\frac{1}{2}\sum_{j=1}^{J}\frac{(x_j - \hat{x}_{ij})^2}{\sigma_j^2}\right]}{\sum_{l=1}^{m} h_l \cdot \exp\left[-\frac{1}{2}\sum_{j=1}^{J}\frac{(x_j - \hat{x}_{lj})^2}{\sigma_j^2}\right]} \tag{6}$$

Note that even before any inferences are attempted, Eq. (6) contains many intuitive insights. The first that should be obvious is that damage predictions for a particular hypothesis that are close to the true damage indicators increase the probability of a given hypothesis. Second, the smaller the variance (i.e., the higher the precision in a measurement) for a given damage prediction, the more weight that surrogate sensor has in the calculation of the posterior for a given hypothesis. This also has the consequence that if the variance is high, the posterior does not shift far from the prior, meaning not much has been learned from the data and model predictions. Further, the more data available for the inferential process, the more weight is given to a particular hypothesis for a given variance. Finally, the effect of the prior is fairly explicit in that it can give more or less probability mass a priori to a particular hypothesis, allowing subjective information or even professional opinions to be taken into consideration. However, if a hypothesis is excluded from consideration, no inferences can be made about said hypothesis. This is equivalent to assigning excluded hypotheses a prior probability of zero.

3 Compartment and Damage Models

In a real fire investigation scenario, there is a need to couple the observed postfire damage signatures to predictions of well-calibrated fire and material degradation models. Fire models can range from relatively simple semi-empirical models and

correlations to physically detailed computational fluid dynamics codes. However, resolving the necessary geometric scales, on the order of millimeters for the flame to meters for the compartment can make computational fluid dynamics codes expensive to implement. Sections 3.1–3.4 introduce a low-order fire evolution model, JT-RISK, as well as a discussion for implementing fire evolution scenarios with secondary ignition criteria in FDS. Simple damage models using the incident heat flux history of a sensor are also discussed.

3.1 Secondary Ignition. The ignition and sustained burning of a material occurs when some critical mass flux of pyrolysate from the material issues forth, burning and sustaining a flame. Because details of the exact ignition process are generally complex, simple ignition models are used throughout the literature. For example, the flux time product model is a semi-empirical model by Shields et al. [20]. Secondary ignition for items in the compartment occurs when the accumulated flux time product exceeds some experimentally determined value if the incident heat flux is greater than some critical heat flux.

For the forward models and experiments considered here, each burner within the room is "instrumented" with devices that measure the incident heat flux. The incident heat flux is then used to inform the ignition of subsequent items in the room using a simple critical heat flux condition. If the incident heat flux to any of the devices for a burner that has yet to ignite is greater than some critical heat flux, then that burner ignites

$$t_{\text{ign},i} = t; \quad q''_{\text{inc}} > q''_{\text{crit},i} \tag{7}$$

3.2 JT-RISK. The JT-RISK model is a simple compartment fire evolution model where combustible items within the compartment burn at specified heat release rates upon ignition. Secondary ignition of combustible materials within the compartment occurs when the ignition criteria are met. The combustible items are rectangular solids with an effective vent at the top and heat flux sensors on four sides. Surrogate sensors that measure incident heat fluxes from the combustible items can also be placed within the compartment and oriented at the users' discretion (see Fig. 2). The incident heat flux to all sensors, including those on the burners, is calculated using the point-source model [21]. The virtual source of the fire is approximated to be the centroid of a conical shell whose height is determined for positive values of Ref. [22]

$$z_{f,i} = 0.23\dot{Q}_i^{2/3} - 1.02D_i \tag{8}$$

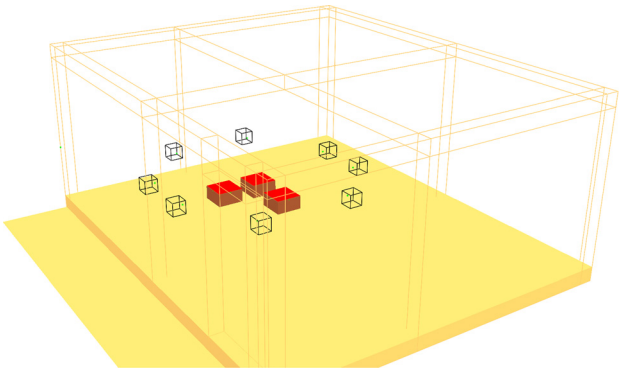

Fig. 2 Three burner hypothesis setup (Sec. 5) rendered using SMOKEVIEW. The rectangular solids in the middle of the figure represent burner objects and are instrumented on four sides with heat flux sensors. Sensors at the periphery represent surrogate sensors and also measure incident heat flux. The same computational domain, with the setup shown in Fig. 3, was used for uncertainty quantification (Sec. 4).

where $z_{f,i}$ is the flame height of fire i in the compartment with HRR, $\dot{Q}_i$, and hydraulic diameter, D_i. The location of the virtual source, $z_{o,i}$, for fire i is then

$$z_{o,i} = z_{c,i} + \frac{1}{3}z_{f,i} \tag{9}$$

where $z_{c,i}$ is the top surface of the rectangular solid. The distance vector from the virtual origin of fire i to some sensor j (be it burner sensor or surrogate sensor) is then

$$\mathbf{d}_{ji} = (x_i - x_j)\hat{\boldsymbol{i}} + (y_i - y_j)\hat{\boldsymbol{j}} + (z_{o,i} - z_j)\hat{\boldsymbol{k}} \tag{10}$$

The incident heat flux to a sensor in the compartment is then

$$q''_j = \sum_{i=1}^{I} \frac{\chi_R \dot{Q}_i}{4\pi||\mathbf{d}_{ji}||^2}\mathbf{n}_j \cdot \mathbf{u}_{ji}; \mathbf{u}_{ji} = \frac{\mathbf{d}_{ji}}{||\mathbf{d}_{ji}||} \tag{11}$$

where χ_r is the radiative fraction of burner i, $\dot{Q}_i$ is the heat release rate of burner i, $\mathbf{n}_j$ is the normal vector defining the orientation of sensor j, and $\mathbf{u}_{ji}$ is the unit vector defining the time-varying direction to fire virtual origin i from sensor j. The ignition of a burner that is not active at the start of a simulation occurs whenever the condition in Eq. (7) is satisfied.

3.3 FIRE DYNAMICS SIMULATOR. FIRE DYNAMICS SIMULATOR is a freely available computational fluid dynamics code that aims to model low-Mach number flow fields by using large eddy simulation to approximate the Navier–Stokes equations [23]. FDS is primarily used in problems that pertain to the dynamics of heat and smoke generated by fires within compartments. There are a number of subgrid models employed that are designed to reduce the computational burden of the fire problem with details available in the FDS technical guide [24]. FDS version 6.7.1 was used with 5 and 10 cm grids to model aspects of an experimental fire compartment and the fire evolution problem.

The surfaces of the compartment and their associated properties are modeled based on the actual components in an experimental burn structure (see Secs. 4 and 5). The walls and ceilings are modeled to behave like 1.6 cm (5/8 in.) thick Type-X gypsum, and the floor is assigned properties of concrete to mimic the concrete pavers present in the burn structure. All boundary vents for the computational domain, except the floor boundary, were "OPEN." A portion of the domain outside of the burn structure door was also included in the computation to more accurately capture in- and outflows through the doorway. Figure 2 shows the three burner setup that will be utilized to exercise the Bayesian framework (details in Sec. 5). Objects in the FDS computational domain are setup in the same way as the JT-RISK model. Combustible items, represented by rectangular solids, have vents at the top and are instrumented with incident heat flux sensors on four sides to determine secondary ignition. A simple directional flame thermometer (DFT) material model is also employed such that the FDS conduction solver, when obtaining surrogate sensor heat fluxes, behaves more realistically. DFTs were utilized in the experimental setup to obtain incident heat fluxes at various locations in the burn structure. Built-in FDS control functions are used to determine when the secondary ignition criterion for a given burner is met.

3.4 Damage. Damage at surrogate sensors within the compartment is calculated using the incident heat flux history. The damage models used are the total energy per unit area (TEA) and a simple Arrhenius damage model.

For the TEA case, the damage at sensor j is modeled as

$$\text{TEA}_j = \int_0^{t_{\text{end}}} q''_{\text{inc},j}\, dt \tag{12}$$

where $q''_{\text{inc},j}$ is the incident heat flux history to sensor j, and t_{end} is the end of the simulation. For the Arrhenius model, the low-order

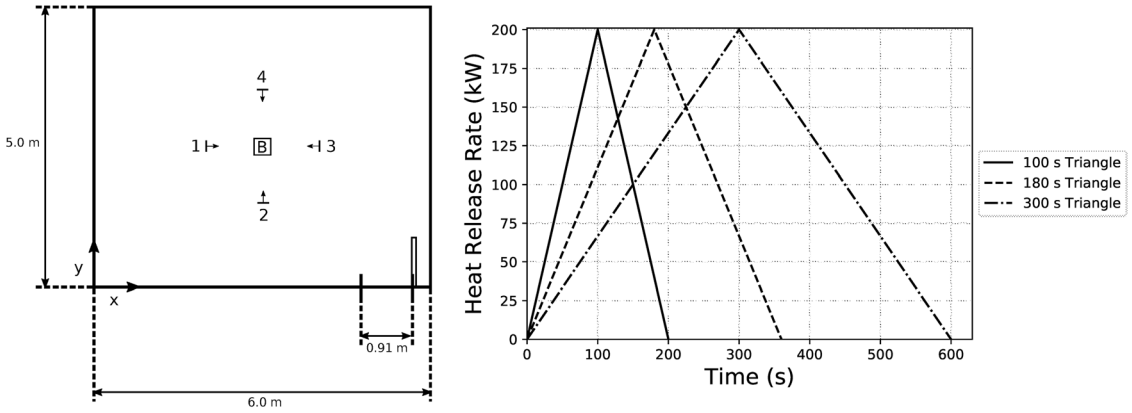

Fig. 3 Compartment setup (*a*) and HRRs (*b*) used for damage model uncertainty quantification for FDS and JT-RISK. Sensors were placed 1 m from the center of the burner on four sides and were situated 0.7 m off the ground.

model is based on work done by Stoll and Greene [25], Moritz and Henriques [26], and Henriques [27] on damage to skin tissue. Anderson and Ezekoye used this model for compartment fire simulations and the same form is used here [28]

$$\Omega_j = \int_0^{t_{\text{end}}} \left(A \cdot \exp\left(-\frac{E}{\bar{R}T} \right) \right)_j dt \tag{13}$$

where A is the pre-exponential, E is the activation energy, $\bar{R}$ is the ideal gas constant, and T is the temporal variation in temperature at the surface of sensor j. To compute the Arrhenius damage, the temperature at the surface needs to be determined from the incident heat flux to the sensor. Two different scenarios corresponding to thermally thin or thick behavior without convective losses are analyzed here. Forms for these equations were taken from Quintiere, and the thick model was modified with a Duhamel integral to account for the transient nature of the incident heat flux [22].

The thermally thin behavior without convective losses has the form

$$T_j = T_0 + \frac{1}{\rho_j c_{p,j} d_j} \int_0^t q''_{\text{inc},j}\, dt \tag{14}$$

where T_0 is the initial temperature, and ρ_j, $c_{p,j}$, and d_j correspond to the density, specific heat, and thickness of sensor j, respectively.

The thermally thick behavior without convective losses takes the form

$$T_j = T_0 + \left(\frac{4}{\pi} \right)^{1/2} \int_0^t \frac{q''_{\text{inc},j}(\tau)}{\left(k_j \rho_j c_{p,j} \right)^{1/2}} \sqrt{(t-\tau)} d\tau \tag{15}$$

where T_0 is the initial temperature, and k_j, ρ_j, and $c_{p,j}$ correspond to the thermal conductivity, density, and specific heat of sensor j, respectively.

4 Uncertainty Quantification

Uncertainty quantification of the damage model predictions and experimental results are necessary to implement the Bayesian methodology outlined in Sec. 2. To quantify the uncertainty in the model predictions, a simple layout consisting of a single burner and four sensors was used. Sections 4.1 and 4.2 describe the test configurations used to conduct the uncertainty analysis as well as results from the models as compared to experimental measurements. The uncertainty analysis for the damage predictions takes the form of a standard error fit, assessing how well the damage predictions from FDS and JT-RISK line up with the experimentally derived damages.

4.1 Test Configurations. Figure 3(*a*) shows the compartment layout of the single burner and four sensors used in experiments, FDS, and JT-RISK. Sensors were symmetrically distributed and placed 1 m from the burner center. For both experiments and FDS, the main door was left open for the tests/simulations. Incident heat flux data at the four sensors were sampled at 1 Hz for the three symmetric triangle fires shown in Fig. 3(*b*). Data were sampled for 200 s, 360 s, and 600 s for the 100 s triangle fire, 180 s triangle fire, and 300 s triangle fire, respectively. For quantifying experimental uncertainty, three replicates were completed for each triangle fire, culminating in nine total experiments.

The TEA and Arrhenius damage models were evaluated, with the Arrhenius damage model evaluated assuming both thin and thick behavior for the sensors. The thermophysical properties of the surrogate sensors were assigned values for wood shown in Table 1 for the Arrhenius damage cases, and the activation energy was scaled by 0.5 to ensure meaningful damage occurred at sensors within the compartment. The thin sensor thicknesses were set to be 0.005 m.

4.2 Results. Replicates of the 300 s triangle fire measured incident heat fluxes are presented in Fig. 4. Similar levels of reproducibility were also observed for the other two triangle fire data sets. Flame leaning toward sensors 1 and 4 was also observed during the experiments, and the result shows up in the increased incident heat flux response at these sensors.

Heat flux results from the 300 s triangle fire are shown in Fig. 5. The top row of subplots for each subfigure corresponds to the measured heat flux at each sensor for experiments (solid line), FDS 2.5 cm (light gray dashed line), FDS 5 cm (dashed line), FDS 10 cm

Table 1 Thermophysical properties of wood taken from various sources

Property	Value
k [29]	1.7×10^{-3} kW/m K
ρ [29]	545 kg/m^3
c [29]	2.385 kJ/kg K
A [30]	6.7×10^8 s^{-1}
E [30]	124.7 kJ/mol

The properties are used to evaluate the thin/thick behavior of the surrogate sensors when considering an Arrhenius damage model.

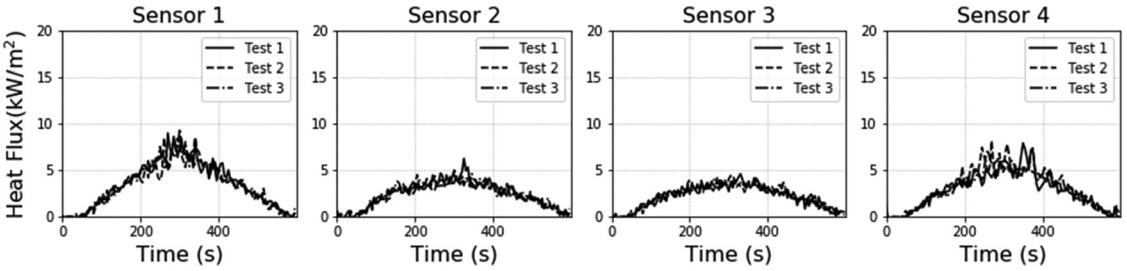

Fig. 4 Experimental heat fluxes measured at the four sensors for three separate tests illustrating test-to-test repeatability. The fires for these three cases all followed the same triangular ramp that peaked at 200 kW, 300 s after ignition.

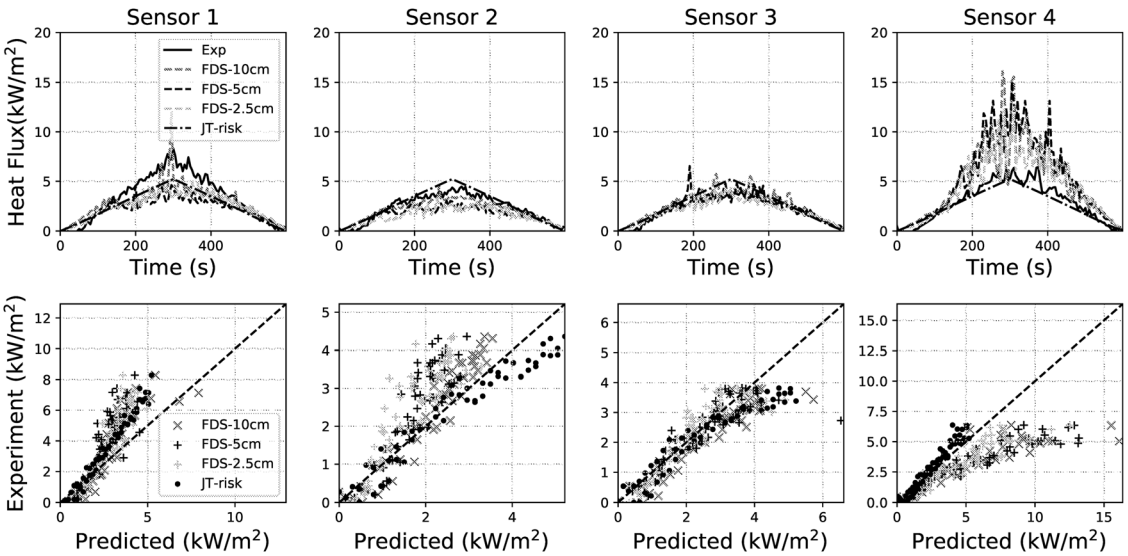

Fig. 5 Experimental and predicted heat fluxes versus time in the top row and scatter of predicted versus experimental heat fluxes in the bottom row for the 300 s triangle fire. In the top row, the solid, dashed, and dashed-dotted lines correspond to experiments, FDS, and JT-RISK, respectively. The gray and black dashed lines correspond to 10 cm and 5 cm grid FDS simulations, respectively. In the bottom row, the + and • signs correspond to FDS and JT-RISK predictions, respectively, with gray symbols corresponding to the 10 cm grid and black symbols corresponding to the 5 cm grid predictions for FDS.

(gray dashed line), and JT-RISK (dashed-dotted line). The bottom row of subplots corresponds to the experimental versus predicted heat fluxes for FDS and JT-RISK for each sensor. Overall there is good agreement between the predicted and measured heat fluxes except for predictions made by FDS at sensor 4. For all three fires, FDS overpredicts the incident heat flux at sensor 4 when the fire reaches its peak. While flame leaning was observed in the experimental tests, it seems that FDS overpredicts this phenomenon resulting in the higher incident heat flux measurements at sensor 4. It is likely that flame leaning is sensitive to fire location, size, and the relative position of the fire to vents in the compartment. For the FDS simulations, positions of the geometry had to be approximated to within 10 cm of the experimental positions due to the snapping behavior of geometry in FDS to the grid resolution. Differences in heat flux measurements between the 2.5 cm and 5 cm cases were relatively small showing convergence of the model at around a resolution of 5 cm (resultant uncertainties in damage were negligible, see Table 2). The 5 cm and 2.5 cm grid resolution simulations took on average about 10 and 30 times longer to compute than the 10 cm cases when comparing total elapsed wall clock time. The 2.5 cm case was run on the University of Texas at Austin Texas Advanced Computing Center Stampede-2 supercomputer and solved using 64 message passing interface processes. The 5 cm and 10 cm cases were completed on a desktop computer with four message passing interface processes. In FDS, the radiation transport equation resolution can also be increased. Radiation transport equation tests were conducted with the 100 s triangle fire case with a grid resolution of 2.5 cm with one simulation having a default resolution of 100 solid angles and the second with a resolution of 700 solid angles. The difference in variation of the incident heat flux measurements for both cases from the mean curve between simulations was less than 5%. The scatter in predictions for a single sensor across tests (not shown here) was consistent for both FDS and JT-RISK.

The measured incident heat fluxes from experiments and computed fluxes from FDS and JT-RISK were used to obtain surface temperature predictions of the surrogate sensors assuming thin and thick behavior for each sensor and each triangle fire tested. From

Table 2 Relative uncertainties for experiments, FDS, and JT-RISK for the three damage models

	TEA	Arrhenius thin	Arrhenius thick
Experiments	4%	3%	4%
FDS 10 cm	25%	18%	17%
FDS 5 cm	32%	20%	21%
FDS 2.5 cm	32%	21%	21%
JT-RISK	17%	12%	12%

Uncertainties were calculated using Eq. (21) for FDS and JT-RISK, and Eq. (22) for experiments.

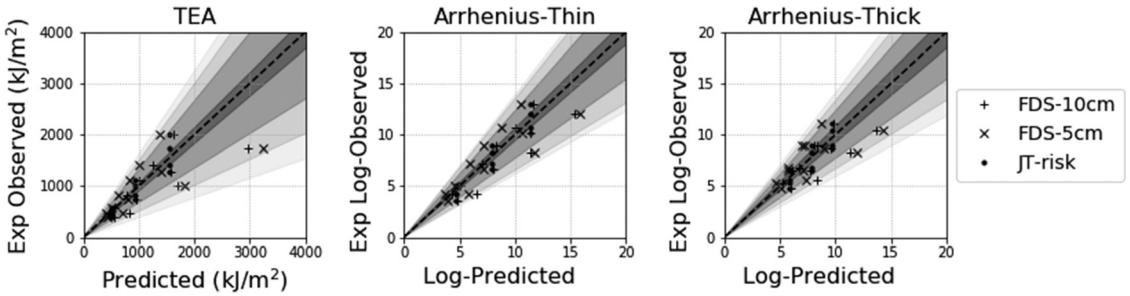

Fig. 6 Experimental damage versus predicted damage for the three damage models: TEA, Arrhenius-thin, and Arrhenius-thick. For the Arrhenius damage models, the logarithm of the damages has been plotted. The +, ×, and • correspond to FDS 10 cm, FDS 5 cm, and JT-RISK predictions, respectively. The darkest gray band represents 95% confidence calculated from propagation of experimental heat fluxes through the models. The gray, light gray, and lightest gray bands represent 95% confidence intervals for JT-RISK, FDS 10 cm, and FDS 5 cm, respectively (see Table 2).

the heat flux and temperature histories from experiments, FDS, and JT-RISK, damages at the surrogate sensors at the end of the simulations were calculated for the TEA, Arrhenius-thin, and Arrhenius-thick cases with FDS 2.5 cm values omitted (Fig. 6).

The damage at the jth sensor for the kth test was defined as follows for the TEA, Arrhenius-thin, and Arrhenius-thick models:

$$x_{jk}^{(\mathrm{TEA})} := \mathrm{TEA}_{jk}$$
$$x_{jk}^{(\mathrm{Thin})} := \log\left(\Omega_{jk}^{(\mathrm{Thin})}\right)$$
$$x_{jk}^{(\mathrm{Thick})} := \log\left(\Omega_{jk}^{(\mathrm{Thick})}\right)$$

The logarithm of the Arrhenius damages is taken because of the exponential nature of the model. To greatly simplify the uncertainty analysis, the errors in predictions by FDS and JT-RISK (denoted with a "hat") are assumed to be iid and normally distributed

$$x_{jk} = \hat{x}_{jk} + e_{jk}; \quad e_{jk} \sim N(0, \sigma_{jk}^2) \tag{16}$$

It is expected that as the value for the predicted damage increases, so does the uncertainty in the predicted value. The standard deviation, σ_{jk}, is therefore assumed to be proportional to the damage

$$\sigma_{jk} = c \cdot \hat{x}_{jk} \tag{17}$$

where c is an as-of-yet unknown constant of proportionality. The likelihood for a single prediction–observation pair is

$$P\left(x_{jk}|\hat{x}_{jk}, c\right) = \left(\frac{1}{2\pi(c\cdot\hat{x}_{jk})^2}\right)^{1/2} \exp\left[-\frac{(x_{jk}-\hat{x}_{jk})^2}{2(c\cdot\hat{x}_{jk})^2}\right] \tag{18}$$

With the iid assumption, the full likelihood for $J=4$ sensors and $K=3$ triangle fires becomes

$$P(\mathbf{x}|\hat{\mathbf{x}}, c) = \prod_{j=1}^{J}\prod_{k=1}^{K}\left(\frac{1}{2\pi(c\cdot\hat{x}_{jk})^2}\right)^{1/2} \exp\left[-\frac{(x_{jk}-\hat{x}_{jk})^2}{2(c\cdot\hat{x}_{jk})^2}\right] \tag{19}$$

$$= \left(\frac{1}{2\pi(c\cdot\hat{x}_{jk})^2}\right)^{JK/2} \exp\left[-\sum_{j=1}^{J}\sum_{k=1}^{K}\frac{(x_{jk}-\hat{x}_{jk})^2}{2(c\cdot\hat{x}_{jk})^2}\right] \tag{20}$$

The estimator $\hat{c}$ that maximizes the likelihood in Eq. (19) is

$$\hat{c}^2 = \frac{1}{JK}\sum_{j=1}^{J}\sum_{k=1}^{K}\left(\frac{x_{jk}-\hat{x}_{jk}}{\hat{x}_{jk}}\right)^2 \tag{21}$$

A similar analysis was completed for the experimental replicates. In this case, because there are multiple replicates for each sensor, the estimator $\hat{c}$ is

$$\hat{c}^2 = \frac{1}{JKL}\sum_{j=1}^{J}\sum_{k=1}^{K}\sum_{l=1}^{L}\left(\frac{x_{jkl}-\bar{x}_{jk}}{\bar{x}_{jk}}\right)^2 \tag{22}$$

Here, $\bar{x}_{jk}$ represents the mean damage at a particular sensor averaged over the three replicates. x_{jkl} represents the damage calculated by propagating a single experimental heat flux through a particular damage model. There are $J=4$ sensors, $K=3$ triangle fires, and $L=3$ replicates. The resultant relative uncertainties calculated for each forward model as well as for each damage model are presented in Table 2. Scatter plots of the experimental versus predicted damages as well as the 95% confidence bands for FDS (light gray) and JT-RISK (gray) are shown in Fig. 6. The dark gray bands represent the 95% confidence interval calculated from experimental replicates.

5 Fire Evolution Configuration

Two sand burners 0.3 m by 0.3 m square by 0.3 m tall constructed in accordance with the *NFPA 286* and one 0.3 m by 0.3 m square by 0.15 m tall gas burner were each electronically controlled using PID mass flow controllers to follow specified HRRs upon reaching some ignition criteria [31]. Each burner was instrumented with four modified DFTs with centers 0.2 m above the ground to measure the incident heat flux in order to determine if the critical ignition heat flux criteria were met. Eight modified DFTs were also placed around the three burner setup, all 0.7 m above the ground to measure incident heat fluxes. The modified DFTs were constructed similarly to standard DFTs (see Ref. [32]) but with a smaller form factor. Construction and calibration of the modified DFTs are discussed in Ref. [33].

Four fire evolution experiments were completed at the burn structure with the compartment configuration shown in Fig. 7. Each burner was assigned a triangular HRR that peaked at 100 kW, 300 s after ignition and decayed to zero 420 s after ignition. Each burner was set to activate if any of the incident heat flux sensors on a burner exceeded 5 kW/m^2. Three of the tests generated experimental data for each of the hypotheses

$$H_1 \equiv \text{Burner 1 initiated the fire evolution} \tag{23}$$

$$H_2 \equiv \text{Burner 2 initiated the fire evolution} \tag{24}$$

$$H_3 \equiv \text{Burner 3 initiated the fire evolution} \tag{25}$$

A separate single test was also conducted to generate the observed, true data for scenario 1 corresponding to

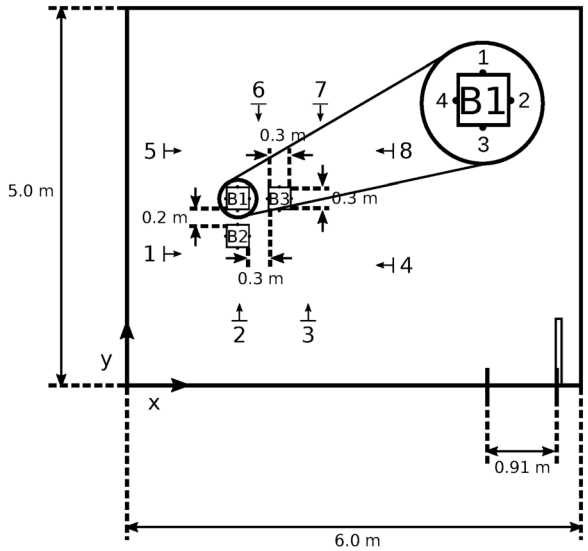

(*a*)

Object	x (m)	y (m)
B1	1.50	2.60
B2	1.50	2.00
B3	2.20	2.60
S1	0.50	1.65
S2	1.40	0.86
S3	2.30	0.86
S4	3.30	1.50
S5	0.50	3.00
S6	1.65	3.70
S7	2.46	3.70
S8	3.30	3.00

(*b*)

Fig. 7 (*a*) Experimental compartment layout for the three burner tests. Burner centroids and sensor locations are shown in (*b*). Arrows on sensors indicate sensing direction. The black numbered dots on the burners represent heat flux sensors that actively monitor for "ignition" based on a particular ignition model. All eight sensors were installed 0.7 m above the ground.

Table 3 Burner ignition times for experiments, FDS with 5 cm grid, and FDS with 10 cm grid

		Experiments (s)	FDS 5 cm (s)	FDS 10 cm (s)
S_1	B_2	119	145 ± 3.3	202 ± 1
	B_3	252	234 ± 8.5	—
S_2	B_1	125	134 ± 24	241 ± 19
	B_3	298	329 ± 36	496 ± 6
S_3	B_1	159	132 ± 10	141 ± 4.8
	B_2	273	210 ± 9.7	249 ± 4.9

The mean and standard deviations were calculated from three replicates for each configuration seeded with different random noise. Two of the three cases for FDS 10 cm, scenario 1 did not ignite.

$$S_1 \equiv \text{Burner 1 initiates the fire evolution} \tag{26}$$

Data from the system were collected at 1 Hz for 720 s for each of the four tests. Spacing between burners varied to ensure burners activated sequentially. The scenarios presented represent a simple set in which the HRR of the involved items, the compartment layout, and the ignition criteria are perfectly known; the only unknown is which scenario produced the observed data.

FIRE DYNAMICS SIMULATOR and JT-RISK were also used to model the setup shown in Fig. 7. Each compartment model was executed three times, one for each of the hypotheses in Eq. (23). FDS computations were completed for grid cell sizes of 10 cm and 5 cm for the three hypotheses (the 2.5 cm predictions were omitted).

Section 6.1 presents the data collected at the surrogate sensors from experiments and compares the results to the predictions made by FDS and JT-RISK. Section 6.2 presents the Bayesian inferential process exercised on the experimental data with FDS and JT-RISK as forward models as well as using the generated experimental data as a forward model (Table 3).

6 Results: Experiments—FIRE DYNAMICS SIMULATOR, JT-RISK

6.1 Data. The burner ignition times for experiments, FDS, and JT-RISK are shown in Fig. 8 for each scenario. JT-RISK burner ignition times for each scenario had better agreement with experiments compared to FDS with a 10 cm grid. Excessive flame leaning was observed in the FDS simulations which is believed to be the main factor in the discrepancy between ignition times for FDS and experiments. Of the three scenarios, scenario 3 had the most

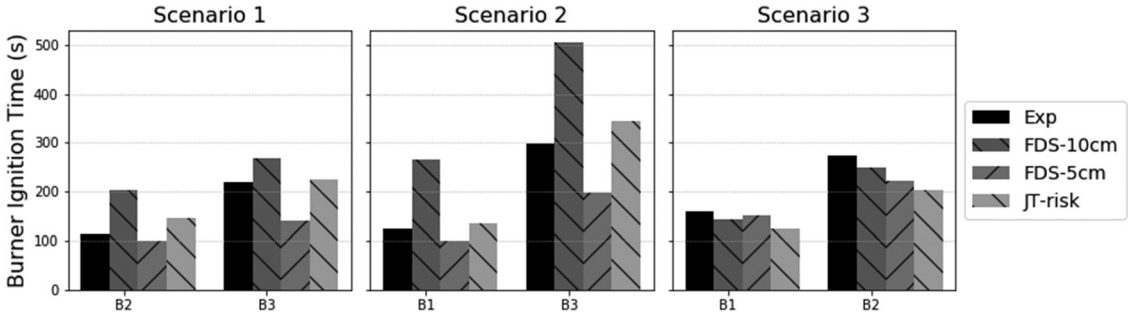

Fig. 8 Comparison of burner ignition times for each scenario. The black, dark gray, gray, and light gray bars represent burner ignition times at each burner for each scenario for experiments, FDS 10 cm, FDS 5 cm, and JT-RISK, respectively.

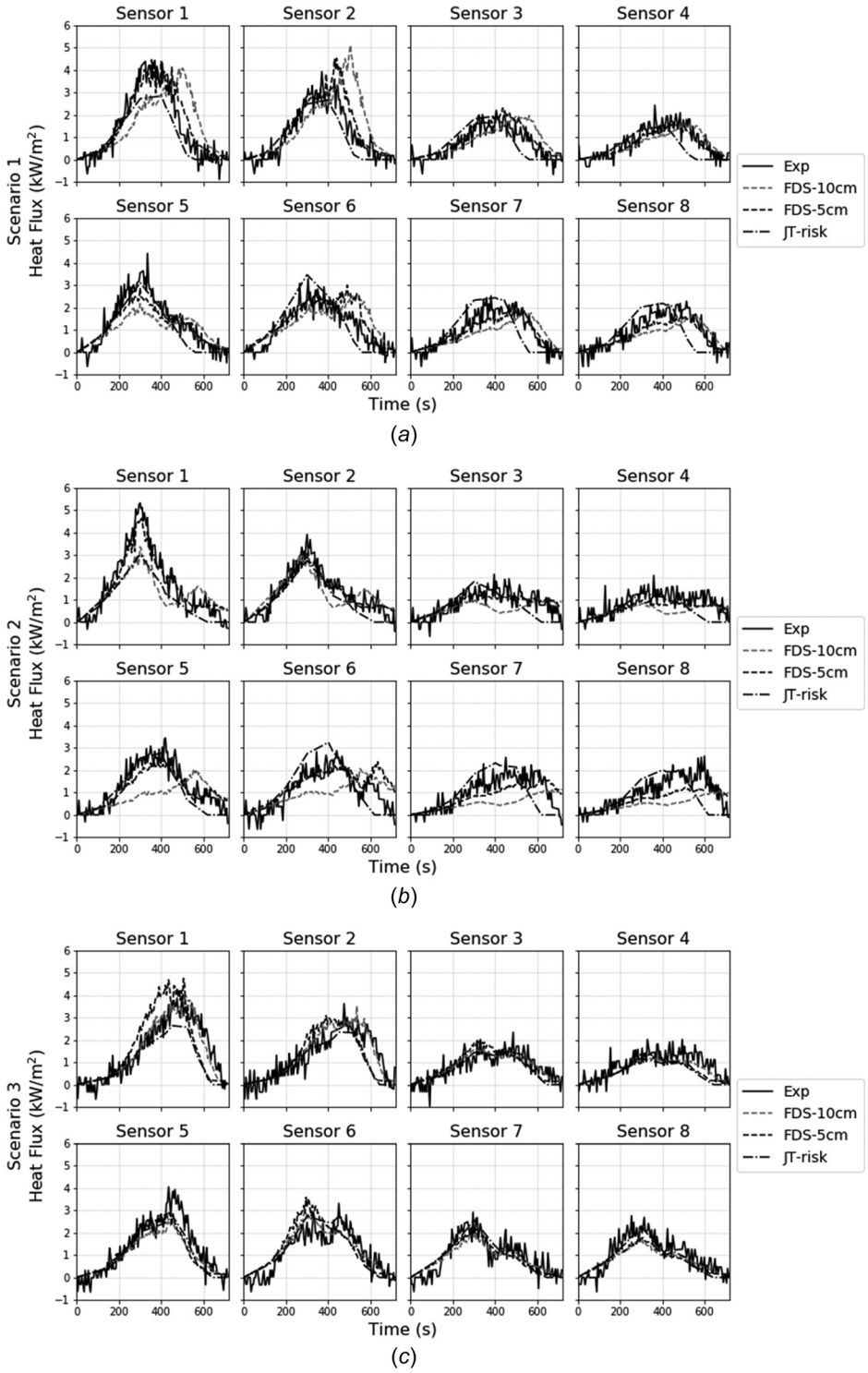

Fig. 9 Incident heat flux versus time for each of the eight surrogate sensors in the compartment for S_1 (*a*), S_2 (*b*), and S_3 (*c*). The solid, dashed, and dashed-dotted lines correspond to experiments, FDS, and JT-RISK, respectively. The gray and black dashed lines correspond to 10 cm and 5 cm grid FDS simulations, respectively. (*a*) Burner 1 ignited first, (*b*) burner 2 ignited first, and (*c*) burner 3 ignited first.

agreement for burner ignition times across experiments, FDS, and JT-RISK.

The incident heat flux at the eight sensors for experiments, FDS, and JT-RISK is shown in Fig. 9 for each of the three scenarios. There is relatively good agreement between the measured heat fluxes and the heat fluxes predicted by JT-RISK for all scenarios as well as for FDS with the 5 cm gird. Because the burner ignition times for FDS 10 cm for scenarios 1 and 2 were grossly overpredicted, the resultant measured heat fluxes at the eight surrogate sensors were poorly predicted. Scenario 3, which had the best agreement between the models and experiments for burner ignition times, also shows good agreement for the incident heat fluxes at the eight sensors.

The incident heat fluxes shown in Fig. 9 were propagated through the three damage models to obtain damages at the surrogate sensors for each scenario, compartment model, and damage

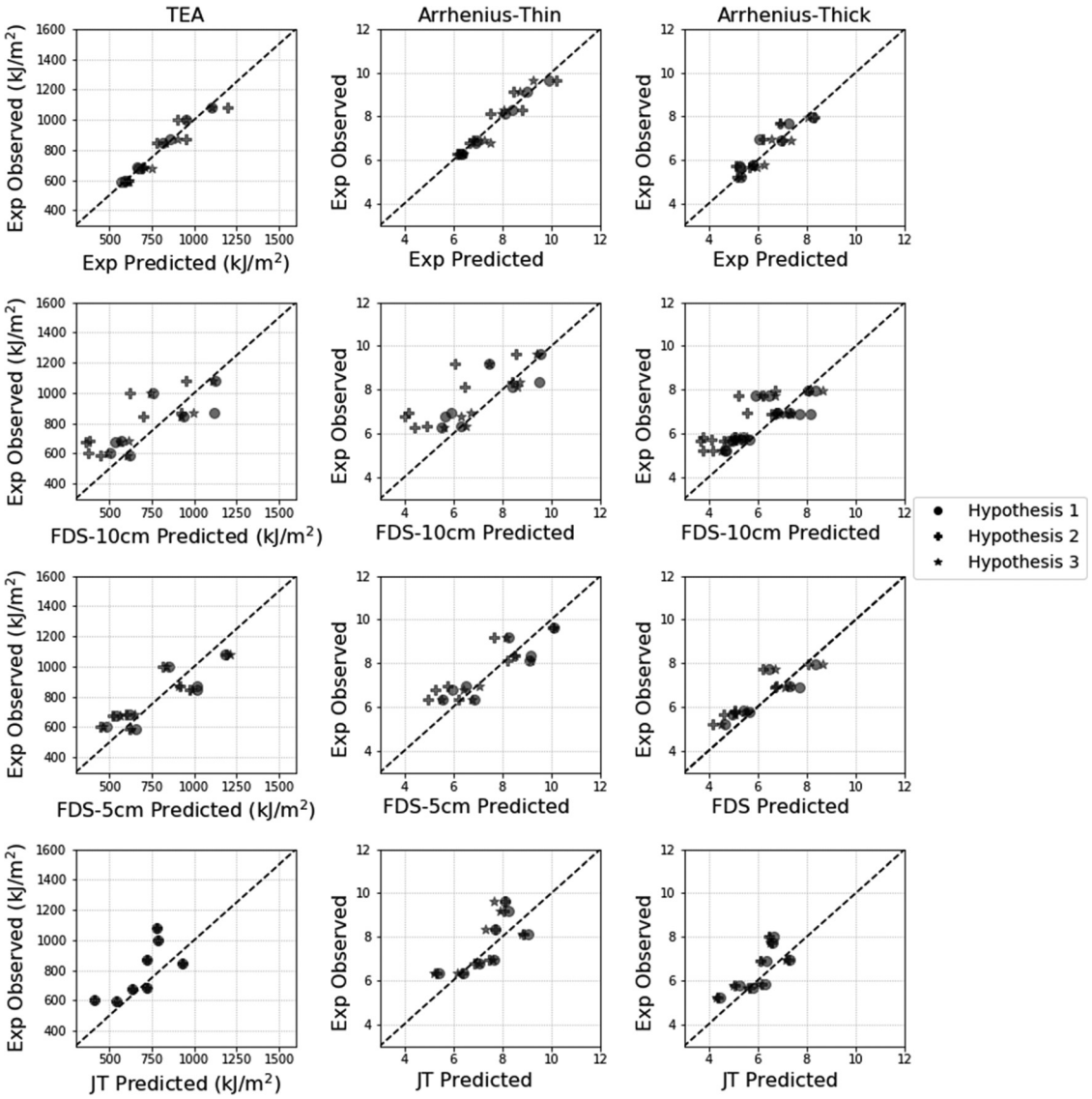

Fig. 10 Scatter plots of predicted damages for each of the compartment evolution models versus experimentally observed damages for the three damage models. The rows represent damage scatter plots using experiments, FDS 10 cm, FDS 5 cm, and JT-RISK as a forward evolution models. The first, second, and third columns correspond to the TEA, Arrhenius-thin, and Arrhenius-thick damage models.

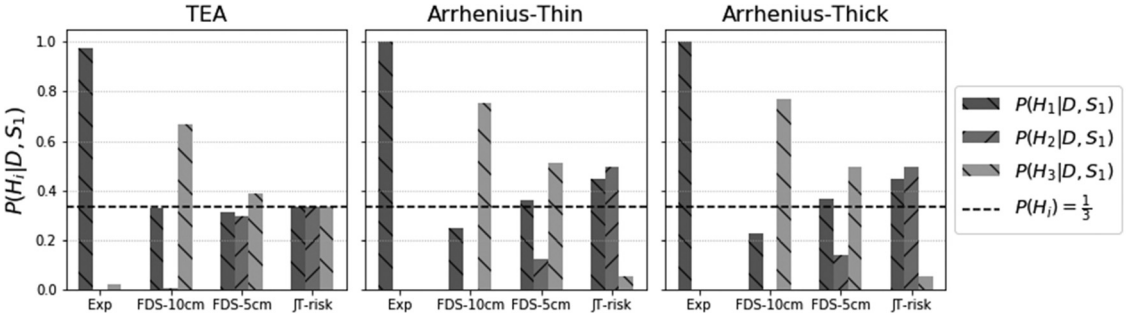

Fig. 11 Hypothesis posteriors for experiments, FDS 10 cm, FDS 5 cm, and JT-RISK for each of the three damage models. The horizontal dashed line represents a flat prior over the three hypotheses of 1/3 (i.e., before observing the data, there is no reason to think any one hypothesis is more true than the others).

model. Scatter plots of the observed, experimental damages for scenario 1 compared to predicted damages made by experiments, FDS, and JT-RISK are shown in Fig. 10 for each damage model and hypothesis.

The first row in Fig. 10 represents using the experimental compartment as a forward model for predicting the observed damages. For the TEA and Arrhenius-thin damage models, the damages derived by testing hypothesis 1 agrees well with the data collected

from scenario 1. A bit more scatter is present for the Arrhenius-thick damage model. Damages from hypotheses 2 and 3 do not agree well with the scenario 1 data across all three damage models. The experimental data show that with a well-calibrated model, the true evolution scenario can be visually elicited.

The second and third rows in Fig. 10 correspond to damage predictions made by propagating the FDS 10 cm and 5 cm incident heat fluxes through the three damage models for each of the hypotheses. These damages are then compared to the experimentally derived scenario 1 data. For all three damage models, the FDS damage predictions do not agree well with the experimentally observed damages for all three hypotheses. Visually, it is difficult to assess which hypothesis corresponds to truth using FDS as the forward compartment evolution model which necessitates application of the Bayesian methodology (Sec. 6.2).

The fourth row in Fig. 10 represents using JT-RISK as a forward model for predicting the observed damages. For the TEA damage model, the JT-RISK compartment evolution model predicts the same damage at each sensor regardless of hypothesis. There is a symmetry present because all three burners ignited in which the total energy released by all three burners for each hypothesis is the same. This symmetry is not present in the Arrhenius damage models, since some of the temporal heating history information is captured by the surface temperature models. Still, the predictions by JT-RISK do not agree well with the observed experimental predictions for all three hypotheses for the Arrhenius damage models. Here, it is also difficult to visually asses which hypothesis corresponds with the truth.

6.2 Bayesian Framework Application. Posterior probabilities for each hypothesis, forward fire evolution model, and damage model are shown in Fig. 11 for scenario 1. The posteriors are calculated using Eq. (6) with the relative uncertainties reported in Table 2 using a flat prior ($P(H_i) = 1/3$). When the experiments are used as forward models, the Bayesian methodology is able to confidently predict the correct hypothesis for all three damage models. This is because the experimental uncertainties presented in Table 2 were small and there was significant variation in damage between hypotheses for a given damage model with the true hypothesis predicting the observed data well.

Both the FDS 10 cm and 5 cm cases fail to predict the correct hypothesis for each of the three damage models, putting more weight in hypothesis 3 than the truth, hypothesis 1. For the FDS cases, it did, however, confidently exclude the possibility of burner 2 starting the fire evolution. For JT-RISK, the TEA damage model did not produce different TEA damages depending on the hypothesis used. For this reason, the posterior and prior probabilities for JT-RISK, TEA are the same (i.e., nothing was learned). For the Arrhenius-thin and thick damage models, JT-RISK predicted the incorrect hypothesis; however, the differences between $P(H_1|D, S_1)$ and $P(H_2|D, S_1)$ were relatively minor. This can be interpreted as that the JT-RISK model confidently excludes the possibility that burner 3 initiated the fire evolution.

It is generally preferable to have a model be less confident and exhibit the kind of behavior that the JT-RISK, TEA damage model exhibited. Having a model be overconfident in the wrong hypothesis might suggest that all uncertainties were not accounted for. For the compartment evolution models presented, the uncertainty in burner-to-burner ignition was not accounted for. It was already shown that the FDS 10 cm case did not predict burner activation well. A separate analysis would need to be conducted to generalize the uncertainty in item-to-item ignition. By including this extra source of uncertainty, it is likely that the model predictions for a given hypothesis will be less confident.

Aside from accounting for other sources of uncertainty, increased model accuracy is desirable. Increasing a compartment model's capability to predict burner-to-burner activation and incident heat flux measurements will reduce the underlying uncertainties with the hope that the models will be able to illicit the truth with confidence.

7 Conclusions

It was shown in this work the development of a Bayesian method for assigning probabilities to items in a compartment that may have initiated the fire evolution within the compartment from analyzing postfire damage metrics to surrogate sensors within the compartment. For the Bayesian method, it was necessary to quantify the uncertainty in forward damage model predictions made by experiments, FDS, and JT-RISK. The large biases observed in FDS heat flux predictions for one of the sensors led to large relative uncertainties for the FDS damage models. It is difficult to pinpoint the source of the modeling bias when the space for user specified parameters in the model is relatively vast and FDS has been shown to predict flame height and plume temperatures well (although validation experiments for actual compartment fires tend to focus on temperature stratification in the compartment and not properties of the fire itself). Uncertainties for experiments were low due to good repeatability with a maximum of 4% relative uncertainty observed for two of the damage models considered. For FDS and JT-RISK, relative uncertainties ranged from 12% for JT-RISK to as high as 32% for FDS.

It was shown that with observed damages generated by an experimental fire compartment, using the same compartment as a kind of forward model proved to make the best predictions of the true fire evolution. The destruction of temporal information by the damage models proved to be challenging for both FDS and JT-RISK. FDS produced relatively overconfident predictions in the wrong hypothesis suggesting the need to incorporate other sources of uncertainty.

While the framework shows promise in the scenarios presented using experiments as a forward model, there is still work to be done in order to use the Bayesian method on true postfire compartments. There is a need, on the experimental side, to accurately measure quantities of interest and another need, on the modeling side, to accurately predict these quantities of interest without needing to simulate all of the detailed physics involved. Accurately quantifying uncertainty is also required throughout to ensure that well-calibrated predictions are made about the hypotheses in question to avoid overconfident predictions in incorrect hypotheses. Model users should take into question all relevant sources of uncertainty when attempting to use models to discriminate between possible hypotheses.

Funding Data

- U.S. National Science Foundation (Award No. 1707090; Funder ID: 10.13039/100000001).

References

[1] NFPA, 2014, "Guide for Fire and Explosion Investigations," National Fire Protection Association, Standard No. NFPA 921.

[2] National Research Council, 2009, "Strengthening Forensic Science in the United States: A Path Forward," National Research Council, Washington, DC.

[3] Gorbett, G. E., and Chapdelaine, W., 2014, "Scientific Method—Use, Application, and Gap Analysis for Origin Determination," International Symposium on Fire Investigation Science and Technology, Sarasota, FL, pp. 3–16.

[4] Cox, A., 2013, "Origin Matrix Analysis: A Systematic Methodology for the Assessment and Interpretation of Compartment Fire Damage," Fire Arson Invest., **64**(1), pp. 1–27.

[5] Gorbett, G. E., Meacham, B. J., Wood, C. B., and Dembsey, N. A., 2015, "Use of Damage in Fire Investigation: A Review of Fire Patterns Analysis, Research and Future Direction," Fire Sci. Rev., **4**(1), p. 4.

[6] Hicks, W., Gorbett, G. E., Kennedy, P. M., Hopkins, R. L., and Abney, W. M., 2006, "Advanced Fire Pattern Research Project: Single Fuel Package Fire Pattern Study," 2006 International Symposium on Fire Investigation Proceedings, National Association of Fire Investigators, Sarasota, FL.

[7] Hicks, W., Gorbett, G. E., Hopkins, M. C., Kennedy, P. M., Hopkins, R. L., and Thurman, J. T., 2008, "Full-Scale Single Fuel Package Fire Pattern Study," 2008 International Symposium on Fire Investigation Proceedings, National Association of Fire Investigators, Sarasota, FL.

[8] Hopkins, R. L., Gorbett, G., and Kennedy, P., 1997, "Fire Pattern Persistence and Predictability on Interior Finish and Construction Materials During Pre and Post Flashover Compartment Fires".

[9] Madrzykowski, D., Fleischmann, C., Hall, J. R., Mitchell, M. R., and Link, R. E., 2012, "Fire Pattern Repeatability: A Study in Uncertainty," J. Test. Eval., **40**(1), p. 104261.

[10] Stauffer, E., 2019, "Interpol Review of Fire Investigation 2016–2019," Forensic Sci. Int., **2**, pp. 368–381.
[11] Wang, J., and Zabaras, N., 2004, "A Bayesian Inference Approach to the Inverse Heat Conduction Problem," Int. J. Heat Mass Transfer, **47**(17–18), pp. 3927–3941.
[12] Biedermann, A., Taroni, F., Delemont, O., Semadeni, C., and Davison, A. C., 2005, "The Evaluation of Evidence in the Forensic Investigation of Fire Incidents (Part I): An Approach Using Bayesian Networks," Forensic Sci. Int., **147**(1), pp. 49–57.
[13] Biedermann, A., Taroni, F., Delemont, O., Semadeni, C., and Davison, A. C., 2005, "The Evaluation of Evidence in the Forensic Investigation of Fire Incidents. Part II. Practical Examples of the Use of Bayesian Networks," Forensic Sci. Int., **147**(1), pp. 59–69.
[14] Nordgaard, A., and Rasmusson, B., 2017, "The Likelihood Ratio as Value of Evidence—More Than a Question of Numbers," Fire Technol., **53**, pp. 301–327.
[15] Overholt, K. J., and Ezekoye, O. A., 2012, "Characterizing Heat Release Rates Using an Inverse Fire Modeling Technique," Fire Technol., **48**(4), pp. 893–909.
[16] Overholt, K. J., 2013, "Forward and Inverse Modeling of Fire Physics Towards Fire Scene Reconstructions," University of Texas, Austin Dissertation.
[17] Overholt, K. J., and Ezekoye, O. A., 2015, "Quantitative Testing of Fire Scenario Hypotheses: A Bayesian Inference Approach," Fire Technol., **51**(2), pp. 335–367.
[18] Kurzawski, A. J., Cabrera, J. M., and Ezekoye, O. A., 2020, "Model Considerations for Fire Scene Reconstruction Using a Bayesian Framework," Fire Technol., **56**(2), pp. 445–467.
[19] Cabrera, J.-M., Moser, R. D., and Ezekoye, O. A., 2019, "A Bayesian Method for Determining the Fire Evolution Within a Compartment," *ASTFE Digital Library*, Begel House, Las Vegas, NV.
[20] Shields, T. J., Silcock, G. W., and Murray, J. J., 1994, "Evaluating Ignition Data Using the Flux Time Product," Fire Mater., **18**(4), pp. 243–254.
[21] Modak, A. T., 1977, "Thermal Radiation From Pool Fires," Combust. Flame, **29**, pp. 177–192.
[22] Quintiere, J. G., 2006, *Fundamentals of Fire Phenomena*, Wiley, West Sussex, England.
[23] McDermott, R., Forney, G., McGrattan, K., and Mell, W., 2010, "Fire Dynamics Simulator 6: Complex Geometry, Embedded Meshes, and Quality Assessment," V European Conference on Computational Fluid Dynamics (ECCOMAS), J. C. F. Pereira and A. Sequeira, eds., Lisbon, Portugal, pp. 1–23.
[24] McGrattan, K., Hostikka, S., McDermott, R., Floyd, J., Weinschenk, C., and Overholt, K., 2013, "Fire Dynamics Simulator, Technical Reference Guide, Volume 2: Verification," NIST Special Publication, Gaithersburg, MD, Report No. 1018–2.
[25] Stoll, A. M., and Greene, L. C., 1959, "Relationship Between Pain and Tissue Damage Due to Thermal Radiation," J. Appl. Physiol., **14**(3), pp. 373–382.
[26] Moritz, A. R., and Henriques, F. C., 1947, "Studies of Thermal Injury: II. The Relative Importance of Time and Surface Temperature in the Causation of Cutaneous Burns," Am. J. Pathol., **23**(5), pp. 695–720.
[27] Henriques, F. C., 1947, "Studies of Thermal Injury V. The Predictability and the Significance of Thermally Induced Rate Processes Leading to Irreversible Epidermal Injury," Arch. Pathol., **43**(5), pp. 489–502.
[28] Anderson, A., and Ezekoye, O. A., 2018, "Quantifying Generalized Residential Fire Risk Using Ensemble Fire Models With Survey and Physical Data," Fire Technol., **54**(3), pp. 715–747.
[29] Incropera, F. P., DeWitt, D. P., Bergman, T. L., and Lavine, A. S., 2007, *Fundamentals of Heat and Mass Transfer*, 6th ed., Wiley, Argonne, IL.
[30] Agrawal, R. K., 1985, "On the Use of the Arrhenius Equation to Describe Cellulose and Wood Pyrolysis," Thermochim. Acta, **91**, pp. 343–349.
[31] NFPA, 2019, "Standard Methods of Fire Tests for Evaluating Contribution of Wall and Ceiling Interior Finish to Room Fire Growth," National Fire Protection Agency, Standard No. NFPA 286.
[32] ASTM, 2016, "Standard Test Method for Measuring Heat Flux Using Directional Flame Thermometers With Advanced Data Analysis Techniques," American Society for Testing and Materials, West Conshohocken, PA, Standard No. ASTM E 3057–16.
[33] Cabrera, J. M., Moser, R. D., and Ezekoye, O. A., 2020, "A Modified Directional Flame Thermometer: Development, Calibration, and Uncertainty Quantification," ASME J. Verif., Validation, Uncertainty Quantif., **5**(1), p. 011003.